The mechano-chemistry of reverse transcriptase

Omri Malik[1,2,#], Hadeel Khamis[1,3,#], Sergei Rudnizky[1] and Ariel Kaplan[1,2,*]

[1]Faculty of Biology, Technion – Israel Institute of Technology, Haifa (32000), Israel
[2]Russell Berrie Nanotechnology Institute, Technion – Israel Institute of Technology, Haifa (32000), Israel
[3]Faculty of Physics, Technion – Israel Institute of Technology, Haifa (32000), Israel
* To whom correspondence should be addressed. Tel:+972-77-8871907; Fax: +972-7708871908; Email: akaplanz@technion.ac.il
# This authors contributed equally to this work

ABSTRACT

Retroviral reverse transcriptase catalyses the synthesis of an integration-competent dsDNA molecule, using as a substrate the viral RNA. Using optical tweezers, we followed reverse transcriptase as it performs strand-displacement polymerization on a template under mechanical force. Our results indicate that reverse transcriptase functions as a Brownian ratchet, with dNTP binding as the rectifying reaction of the ratchet. We also found that reverse transcriptase is a relatively passive enzyme, able to polymerize on structures templates by exploiting their thermal breathing. Finally, our results indicate that the enzyme enters the recently characterized backtracking states from the pre-translocation complex.

INTRODUCTION

The virally-encoded reverse transcriptase (RT) is responsible for genome replication in retroviruses. RT is a DNA- and RNA-dependent DNA polymerase that catalyses the synthesis of an integration-competent dsDNA molecule. RTs have the “right hand” structure typical of cellular DNA polymerases, with palm, fingers and thumb subdomains, and also a spatially separated RNase H domain[1]. Using both steady state and pre-steady state techniques[2–7], previous studies have described a mechanism of polymerization by RT, which is similar to the mechanism of other DNA polymerases. However, the rates of polymerization by RTs are fairly slow and their processivity is poor relative to other DNAPs[8]. In addition, as opposed to most (but not all[9–13]) DNAPs, which require a single strand DNA (ssDNA) template, RT is capable of efficiently unwinding duplexes in the template during polymerization. This strand displacement (SD) synthesis activity by RT is required for the polymerization on the highly structured vRNA[14] , the removal of RNase H resistant RNA fragments[15] and polymerization on the long terminal repeats[16]. Importantly, although the rates of both displacement and non-displacement DNA synthesis vary for different sites over the template, SD synthesis is, on the average, slower by a factor of 3–4[17], as compared to primer extension synthesis.

Remarkably, although numerous structural and biochemical analyses have been performed to elucidate the mechanisms governing dNTP binding[18,19], induced conformational change[20–22] and catalysis[23,24], much less is known about the mechanisms and kinetics of RT’s translocation. The first question that needs to be answered in order to incorporate the translocation step into the enzyme’s cycle, is what is the location of the translocation step in the order of events that comprise a nucleotide addition step. Single molecule methods have been implemented to dissect the mechano-chemical cycle of RNA and DNA polymerases by using mechanical force to assist or inhibit translocation[25]. For instance, the location of the translocation step for Phi29 DNA polymerase and Escherichia coli RNAP was found to take place after pyrophosphate (PPi) release and prior to dNTP binding[13,26]. Next, the *mechanism* of translocation needs to be elucidated. Two alternative mechanisms have been proposed: a “powerstroke” (PS) mechanism, where a certain chemical step

(dNTP hydrolysis or PPi release) directly power translocation [76], and a "Brownian Ratchet" (BR) mechanism where the enzyme moves back and forth between the pre- and post-translocation state, driven by thermal energy, and a chemical reaction traps the post-translocation configuration, driving the reaction forward. Interestingly, despite the paucity of experimental data, some controversy exists regarding the mechanism of translocation by RT. An active, PS model is supported by previous studies showing that nucleotide binding is associated with displacement of the highly conserved YMDD motif that is part of the enzymes active site[27]. Release of this "loaded spring" following catalysis may provide the drive for the translocation reaction. However, a Brownian ratchet model of translocation is supported by biochemical studies using site-specific footprinting[28], which support the existence of a translocation equilibrium, in which RT rapidly oscillates between two states, and dNTP binding acts as the pawl of a ratchet. This type of mechanism was demonstrated for RNA polymerase[29], as well as for the replicative Phi 29 DNA polymerase[13]. Finally, given that RT is not stalled by duplexes in its template, it is necessary to clarify how RT copes with the obstacle presented by the duplex DNA. Generally, unwinding of nucleic-acid duplexes by enzymes, such as helicases, has been described by two extreme models[30]: In an "active" model the enzyme unwinds the nucleic acid duplex by directly destabilizing the hairpin fork. In contrast, in the "passive" model, the enzyme is unable to destabilize the duplex ahead, but it exploits the spontaneous, thermally-driven opening of the duplex (thermal "breathing"). These are extreme mechanisms, and most enzymes will share some of the properties of both, i.e. will partially destabilize the duplex ahead, but will still be affected by the duplex spontaneous breathing[31,32]. Taken together, the location of the translocation step, the mechanism of translocation and the mechanism of duplex unwinding determine, together, how RT responds to changes in [dNTP] and to the presence and magnitude of an external force. Hence, experimentally characterizing these responses can shed light on the mechano-chemistry of RT.

Here, we use optical tweezers to elucidate the mechanism of translocation Moloney Murine Leukemia Virus (M-MLV) RT. By following strand-displacement polymerization by RT on a DNA hairpin, and separating active polymerization phases from pauses, we were able to characterize the force- and nucleotide-dependence of RT's velocity, and compare these dependencies with the predictions of detailed kinetic models. Furthermore, we show that a comparison of the experimentally measured density of pauses with the predictions of the kinetic models provides a powerful tool to discriminate between plausible models, identify the kinetic step from which RT enters the pauses, and calculate the intrinsic rate of pausing by RT.

RESULTS

Processive polymerization by M-MLV Reverse Transcriptase is force- and [dNTP]-dependent

We followed SD polymerization by RT on a 265 bp DNA hairpin, that is attached to two ~ 600 bp dsDNA handles (Fig. 1A). Each handle harbors a tag (biotin and digoxigenin, respectively), allowing to tether the complete construct between two microspheres trapped in the two separate optical traps of a dual-trap high resolution optical tweezers (Fig. 1A). As shown previously[33], upon exposure of the complex to a mixture of RT an dNTPs, RT binds to the DNA construct by using the 3'-OH terminus of the dsDNA handle as a primer and engages in SD polymerization of the hairpin. SD polymerization results in an increase in the tether extension, by an amount equal to the addition of a single bp and a single nt for each catalytic cycle. With the known mechanical response of dsDNA and ssDNA, these extension changes can be translated into the number of bp polymerized (Figure 1B). We recently showed, that polymerization is punctuated with numerous inactive phases, and that that most of them represent backtracking of the polymerase[33]. Here, we take advantage of our ability to reliably separate the pauses, and concentrate on the active phases of polymerization. Hence, we measure the pause-free velocity for different forces (4-16 pN) and a broad range of [dNTP] (0.5 – 250 μM). Fitting the data collected for each force indicates that, for all forces probed, the velocity follows Michaelis-Menten (MM) kinetics, $V = V_{max}([dNTP]/(K_M + [dNTP]))$, where V is the pause free velocity (Figure 2A). Moreover, the

data shoes that V_{max} is a sensitive function of force (Fig. 2B), exhibiting a nearly 3-fold increase as the force is increased from 4 to 16 pN. The uncertainty in the determination of K_M is too large to determine its force-dependence, likely because of the difficulty of accurately characterizing the velocity at low force and [dNTP].

Mechano-chemical models for SD polymerization make distinct predictions for the dependence on force and [dNTP]

In order to extract from the data information about the translocation step during RTs polymerization reaction, we need to analyze how force affects the mechano-chemical cycle. Note, that previous studies have used an external force directly acting on a molecular motor to extract this information. Here we show that, for an enzyme capable of performing SD polymerization, modulating the strength of the barrier imposed by the duplex ahead can fulfill a similar role.

Previous studies have delineated the elongation kinetic cycle of RT and other DNA polymerases as follows: Following binding of a new nucleotide, the complex undergoes a structural transition involving a hinged movement of the fingers domain and other smaller movements, from an "open" conformation which allows binding of nucleotides and, possibly, movement of the polymerase on the DNA, into a "closed" conformation that ensures proper positioning of the 3' end of the primer, the template and the incoming nucleotide as if they were already in a dsDNA conformation. Next, a phosphodiester bond is formed, followed by a second structural transition ("opening" of the fingers). Finally, the pyrophosphate is released. Since with our experimental conditions PPi release is an irreversible transition ([PPi]≈ 0), this cycle can be simplified to include a nucleotide binding step, a catalysis step and a PPi release step, as follows[34,35] :

$$RD_n \underset{k_{-b}}{\overset{k_b[T]}{\leftrightarrow}} RD_nT \xrightarrow{k_c} RD_{n+1}PP_i \xrightarrow{k_p} RD_{n+1} + PPi \qquad (1)$$

Here, R represents the RT enzyme, D is the DNA strand being synthesized, of size n, and T the incoming dNTP. However, in addition to the chemical steps described above, being RT a processive enzyme that can perform successive incorporations without dissociation, there must be also a mechanical step of translocation, where RT moves by one bp on its template strand. As detailed above, this mechanical step may be located at different positions in the above cycle, and the mechanism underlying this step may correspond to either a PS or a BR model. Importantly, for both mechanisms, the end point of the reaction is progress along a chemical as well as a mechanical reaction coordinate. However, while for the PS mechanism translocation is tightly coupled to a specific chemical step, such us PPi release, and therefore can be represented by a diagonal movement in the two-dimensional energy landscape (Fig. 3B,D), for BRs the movement between the pre- and post-translocation positions precedes the chemical step and the system moves in two orthogonal steps in its energy landscape (Fig. 3A,C): first along the mechanical coordinate, and then along the chemical one. This indicates that a PS mechanism should be integrated into the mechano-chemical cycle by considering a specific chemical step as a mechano-chemical step. For example, if translocation takes place with release of PPi, via a PS mechanism, we will simply consider k_p to be a step that includes both PP_i release *and* translocation. Alternatively, formulating a BR model requires an additional, purely mechanical step to be added to the cycle, preceding the chemical step that rectifies the spontaneous fluctuations (the "pawl" of the ratchet). Hence, if translocation takes place via a BR rectified by PPi release, we add a pure translocation transition, with forward and backwards rates k_t, k_{-t} , between $k_c$and k_p.

In the special case of SD polymerization, when unwinding of the substrate is coupled to polymerization, translocation requires an open fork, i.e. a ssDNA region equal or greater than the enzyme's step size. Hence, we treat the open fork as a "substrate" of the translocation reaction and

write the translocation step as $R_m \underset{k_{-t}}{\overset{k_t P_{open}}{\leftrightarrow}} R_{m+1}$, where P_{open} is the "concentration" of open forks, i.e. the probability for the fork to be open by at least the size of the enzyme's step. As shown in the Supplementary Discussion, P_{open} depends on the free-energy difference between open and closed states, and is modulated by an external force applied on the hairpin, which stabilizes the open state. In addition, if the enzyme is not completely passive there will be some degree of destabilization of the closed state, given by a change in the free energy ΔG_{RT}. Hence, both the force and ΔG_{RT} can modulate the translocation step. However, how this affects the overall rate of polymerization depends on the specific model for the mechano-chemical coupling that describes RT.

The first mechano-chemical model we consider is a BR where the rectification is provided by dNTP binding (BR/B model, Fig. 3A), as was previously suggested[28,36], and demonstrated for other polymerases[26,29]. Such model can be described by the following reduced scheme:

$$R_n D_n \underset{k_{-t}}{\overset{k_t P_{open}}{\leftrightarrow}} R_{n+1} D_n \underset{k_{-b}}{\overset{k_b [T]}{\leftrightarrow}} R_{n+1} D_n T \overset{k_c}{\rightarrow} R_{n+1} D_{n+1} P_i \overset{k_p}{\rightarrow} R_{n+1} D_{n+1} \tag{2}$$

Previous studies have suggested that the rate limiting step in the cycle of DNAPs is the conformational change required for catalysis[2,35,37–39]., and that both pyrophosphate release and translocation[2,38,40] are fast. This is also the case for RT, at least for its DNA-dependent synthesis activity[9–11]. Hence, assuming that catalysis is the rate limiting step, i.e. $\mathrm{k_c} \ll \mathrm{k_p}, \mathrm{k_{-b}}, \mathrm{k_{-t}}$, we can show (Supplementary Information) that, the polymerization velocity follows MM kinetics with $\mathrm{V_{max}} = \left[\frac{1}{\mathrm{k_c}} + \frac{1}{\mathrm{k_t P_{open}}}\right]^{-1}$ and $\mathrm{K_M} \approx \mathrm{K_D} \frac{1+\frac{\mathrm{K_\delta}}{\mathrm{P_{open}}}}{1+\frac{\mathrm{k_c}}{\mathrm{k_t P_{open}}}}$,

where we have introduced the notation $K_\delta \equiv \frac{k_{-t}}{k_t}$, and $K_D \equiv \frac{k_{-b}}{k_b}$. Three more models are considered (Fig. 3B-D and Supplementary Discussion): In a second BR model, the enzyme alternates between pre- and post-translocation after catalysis, and is rectified by the release of PPi (BR/R model). The last two additional models invoke a PS mechanism: In the first, translocation is coupled with binding of dNTP (PS/B model), and in the second it is coupled to the release of PPi (PS/R model). All the models predict MM kinetics, with parameters V_{max} and K_M that can be explicitly calculated (Supplementary Discussion, and Supplementary Tables 4). Notably, the models predict a different force dependence for the kinetic parameters, V_{max} and K_M, as summarized in Table 1.

As these models have different predictions for the dependence of the kinetic parameters on P_{open} and therefore on the applied force and ΔG_{RT}, our measurements should help us elucidate which is the appropriate model to describe RT. In fact, they immediately rule out one of the models analyzed, PS/B, which predicts a force-independent V_{max}, in disagreement with the monotonically-increasing dependence shown in Fig. 2B. The three other models we consider all predict a V_{max} that increases with force, and are consistent with the measurements. Unfortunately, the uncertainty in the determination of K_M is very large, thus preventing a significant discrimination between these models, which have different predictions for the force dependence of K_M. However, as we show below, RT's pausing phenotype will help us clarify this point.

The mechano-chemical models predict the force- and [dNTP]-dependence of the pause density, and provide a constrain on the mechanism of polymerization

In our previous work, we showed that processive SD polymerization by M-MLV RT is punctuated with pauses, and that most of these pauses are backtracking events, at which the enzyme misses alignement with the 3'OH terminal of the primer. Notably, although pauses are off-pathway from

the main polymerization cycle, a complete characterization of RT's mechano-chemical cycle must incorporate the steps leading to the paused state. Hence, using the kinetic models of Fig. 3, we develop expressions for the Pause Density (PD), defined as the number of pauses per enzymatic cycle or, equivalently, the number of pauses per polymerized bp. We define PD_j as the probability, per cycle, to enter a pause from state j, where j is a number characterizing the position of a state in the cycle. So, for example, while state 1 is always the pre-translocated enzyme with no dNTP bound, the identity of state 2 can vary: for model BR/B is the post-translocation state, with no dNTP, and for model PS/B is the post-translocated enzyme with dNTP bound. PD_j can be calculated by examining the rate of entering the paused state from state j vs. the rate of productively continuing the cycle. The latter is given by k_j^{net} and therefore:

$$PD_j = \frac{k_{pause}}{k_{pause} + k_j^{net}}$$

where k_{pause} is the intrinsic rate of entering the pause. Hence, to calculate PD_j we calculate k_j^{net} for a specific state of origin and a specific mechano-chemical model. For example, in the case of model BR/B, the pause can be entered from 4 different kinetic states (Fig. 3): i) the pre-translocation state, ii) the post-translocated state (before dNTP binding), iii) the dNTP bound, post-translocated state, and iv) the post-catalysis state, before PPi release. It can be shown (Supplementary Information) that under the assumptions that k_c is the rate limiting step,

$k_1^{net} = k_t P_{open} \left[\left(1 + \frac{k_{-t}}{k_c}\frac{K_D}{[T]}\right)\right]^{-1}$, $k_2^{net} = \frac{k_b[T]k_c}{k_c+k_{-b}} = \frac{[T]}{K_D}k_c$, $k_3^{net} = k_c$, and $k_4^{net} = k_p$.

As can be seen, pauses originating from different states in the mechano-chemical cycle will exhibit a different force and [dNTP] dependence. Specifically, for the BR/B model, PD_1 depends on both force and [dNTP], PD_2 only on [dNTP], and $PD_{3,4}$are force- and [dNTP]-independent. In the same way, we calculate the predicted PDs for the rest of the models, and for each potential state of origin for the pauses within their mechano-chemical cycle (Supplementary Discussion, Supplementary Table 5). Their dependence on force and [dNTP] is summarized in Table 2.

Our previous work showed that PD decreases as both force and [dNTP] are increased. Hence, the analysis presented above indicates that the only models compatible with the PD data are models BR/B and PS/B, and in both cases the pauses must originate from the first state in the cycle: the pre-translocated state. However, we showed above that PS/B is not compatible with the pause-free velocity data, since it predicts a force-independent Vmax. Hence, the only model which is compatible with both the velocity data and the pausing data, is model BR/B. We conclude that RT is a BR, rectified by dNTP binding, and that backtracking pauses are accessed from the pre-translocation state.

RT is a relatively passive enzyme

Having established the architecture and mechanism of the mechano-chemical cycle of RT, we use our data to elucidate also the mechanism of strand displacement. Note, that since all the parameters affecting P_{open} ,with the exception of ΔG_{RT}, are measured, we can consider P_{open}, for our specific experimental setup, to be a function of ΔG_{RT} only (Supplementary Discussion). Hence, we fit the expressions we found for V_{max} (as a function of force) and PD_1 (as a function of force and [dNTP]), to our experimental data (Supplementary Fig. 2), to find ΔG_{RT} and the microscopic rate constants governing the mechano-chemical cycle. As shown in Table 3, our data shows that, during SD polymerization, RT is a moderately passive enzyme, destabilizing the fork only by ~ $1k_BT$.

DISCUSSION

In this work, we followed SD polymerization of RT on a DNA template at the single molecule level. Separating the active phases of polymerization from the pauses induced by backtracking of the enzyme, we were able to characterize the pause-free velocity of RT in a broad range of mechanical and chemical conditions. We found that RT exhibits MM kinetics at all forces probed, and that the resulting V_{max} is a monotonically increasing function of the force applied on the duplex DNA. We postulated different kinetic models for the translocation, and derived the expected kinetic parameters for all of them. Comparing the predictions of these models with the force dependence of V_{max} enabled us to rule out one of the models. Next, we derived predictions for the pause density, for each of the kinetic models and for each of the possible states from which pauses are accessed, and compared the predictions of these models with the dependence of PD on force and [dNTP], as reported in our previous work[33]. This allowed us to determine that only one model is compatible with both the pause-free velocity and the PD data, and to conclude that RT uses a BR mechanism, where binding of a new dNTP acts as the rectifier of translocation.

Interestingly, although our findings on the mechanism of translocation are in agreement with some previous studies[28], they disagree with others: Structural studies have suggested that RT translocation takes place by a PS model, and It was suggested that the conserved YMDD motif "buffers" the energy from dNTP binding as mechanical strain which powers translocation upon release[27]. However, as translocation is an inherently mechanical process, its reliable characterization requires mechanical means, i.e. the application of force.

Previous single molecule studies of RNA and DNA polymerases have used similar approaches as ours, based on globally fitting the data to a force-dependent model[13,26]. However, their approach was to study translocation under a force that directly opposes (or facilitates) the enzyme movement. Hence, this necessitates attaching the enzyme to one of the beads (or to a surface), a procedure that may affect its activity in unknown ways. Here we show that, by considering the fork as an energetic barrier for translocation during SD synthesis, we can extract the same type of information as these previous works did for other enzymes. Therefore, we suggest that this approach may be of use to study the mechano-chemistry of other SD competent polymerases.

Recently, we showed that strand displacement by RT is dominated by its pausing kinetics, were inactive states during processive polymerization are the result of backtracking of the enzyme. In addition, we postulated that residues in the protein (which we collectively called the "anchor domain", AD) make contact with ssDNA ~8 bp ahead of the fork, stabilize the enzyme and prevent backtracking. Here, we showed that backtracking pauses are accessed from the pre-translocation state, in line with backtracking of RNAP[29].Further studies will be required to elucidate the coupling of the AD movement with the mechano-chemical cycle of polymerization.

Finally, our results also indicate that the destabilization of the fork by RT is very small, ~1 kBT, and are consistent with previous results for HIV-1 RT[31]. This relative "passiveness" is what makes the velocity of RT highly sensitive to the *presence* of a duplex. However, RT is expected to be affected also by the *nature* of the structural motifs it encounters in its template. Our experiments indicate that the velocity of RT is reduced by more than 3-fold, when the force is reduced from 16 to 4 pN. Hence, a similar modulation is expected when RT encounters structural elements whose stability spans a similar range, providing a mechanical basis for the modulation of RT by structural elements in the vRNA. Interestingly, the strongest structural motifs present in the HIV-1 genome are the TAR elements[14], which have been shown to unfold at ~ 15 pN in an optical tweezers experiment. Hence, it is tempting to speculate that RT and its vRNA substrate have co-evolved to allow for an efficient and potent regulation of reverse transcription.

MATERIALS AND METHODS

Molecular constructs for single molecule experiments

The DNA sequences used as a polymerization template (Supplementary Table 1) was amplified by PCR from a plasmid that was a generous gift from Daniela Rhodes (MRC, Cambridge, UK)). Primers used for the amplification reactions are listed in Supplementary Table 2. The constructs were digested using DraIII-HF (New England Biolabs) overnight according to the manufacturer's instructions. A 10 bp hairpin (Sigma) was ligated to the construct using T4 DNA ligase (New England Biolabs), in a reaction with 1:10 molar excess of the hairpin, at 16 °C. The construct was subsequently digested overnight with BglI (New England Biolabs). Two 600 bp DNA handles, each incorporating a specific tag (digoxigenin and biotin), were generated using commercially purchased 5' modified primers (Supplementary Table 3) in a standard PCR reaction. Two of the primers were designed to contain repeats of three DNA sequences recognized by single strand nicking enzymes: Nt.BbvCI and Nb.BbvCI (both from New England Biolabs) on the biotin-tagged handle and on the digoxigenin-tagged handle, respectively. The nicking enzymes generated 29 nt complementary overhangs on each handle. Handles were mixed at equal molar ratios for DNA annealing, creating a ~1200 bp fragment of annealed DNA handles. The polymerization templates were ligated to the DNA handles using a rapid ligase system (Promega) in 3:1 molar ratio, 30 min at room temp.

Reagents

M-MLV RT and dNTPs were purchased from New England Biolabs and Sigma, respectively.

Optical Tweezers

Experiments were performed in a custom-made double-trap optical tweezers apparatus, as previously described[33,41]. Briefly, the beam from a 852 nm laser (TA PRO, Toptica) was coupled into a polarization-maintaining single-mode optical fiber. The collimated beam out of the fiber, with a waist of w_0=4mm, was split by a polarizing beamsplitter into two orthogonal polarizations, each directed into a mirror and combined again with a second beamsplitter. One of the mirrors is mounted on a nanometer scale mirror mount (Nano-MTA, Mad City Labs). A X2 telescope expands the beam, and also images the plane of the mirrors into the back focal plane of the focusing microscope objective (Nikon, Plan Apo VC 60X, NA/1.2). Two optical traps are formed at the objective's focal plane, each by a different polarization, and with a typical stiffness of 0.3-0.5 pN/nm. The light is collected by a second, identical objective, the two polarizations separated by a beamsplitter, and imaged onto two Position Sensitive Detectors (First Sensor). The position of the beads relative to the center of the trap is determined by back focal plane interferometry[42]. Calibration of the setup was done by analysis of the thermal fluctuations of the trapped beads[43], which were sampled at 100kHz.

Single molecule polymerization experiments

The full polymerization construct was incubated for 15 min on ice with 0.9 µm polystyrene beads (Spherotech), coated with streptavidin (SA), and diluted 1000-fold in RT buffer (RTB; 50 mM Tris-HCl, 75 mM KCl, 3 mM MgCl2, 10 mM DTT, pH 8.3 @ 25°C). The SA beads bound to the DNA constructs, together with 0.9 µm anti-digoxigenin (αD) coated beads were introduced into the microfluidic channel filled with RTB. Tether formation was performed *in situ* (inside the experimental chamber) by trapping a SA coated bead in one trap, trapping an αD bead in the second trap, and bringing the two beads into close proximity to allow binding of the digoxigenin tag in the DNA to the αD in the bead. After a few seconds, the beads were moved away from each other while monitoring changes in the force. Establishment of a tether is indicated by an increase in force as the traps are separated. In some of the experiments, the polymerization reaction was initiated by flowing activity buffer (RTB with the addition of 1-250 uM dNTP and 200U/ml RT) into the chamber. In other experiments, a laminar flow chamber (u-Flux, Lumicks) was used, with one channel containing RTB and a different one activity buffer. Polymerization was initiated by moving the beads into the activity buffer channel.

Experiments were conducted in a semi-passive mode, in which polymerization takes place with no feedback on the force but where, if the force exceeds a predetermined value, the position of the steerable trap is rapidly changed in a single step and in a direction and magnitude that are expected to restore the measured force to the range of forces that were pre-established (typically, ±1.5 pN of the nominal force). As a result, our polymerization data consists of intervals of passive-mode operation, that are separated by sudden "jumps" in the position of the steerable trap. Segments in the data during which the mirror moves were identified and subtracted from further analysis.

Data analysis

Conversion of the data into physical units. Data were digitized at a sampling rate fs=2500 Hz, and saved to a disk. All further processing of the data was done with Matlab (Mathworks). Using the calibration parameters previously obtained, the total extension of the tether, x, and the force acting on it, F, were calculated. From the extension *vs*. time traces, we identified the sections in the data containing SD polymerization. Then, the number of bp polymerized during SD and PE activity (N_{SD} and N_{PE}, respectively), were calculated as:

$$N_{SD}(t) = \frac{x(t) - N_H \cdot d_{ds} \cdot f_{ds}[F(t)]}{d_{ds} \cdot f_{ds}[F(t)] + d_{ss} \cdot f_{ss}[F(t)]}$$

where N_H=1200 is the number of bp in the dsDNA handles, N_{HP} is the number of bp in the hairpin, $d_{ds} = 0.34\ \mathrm{nm}$ the rise per bp for dsDNA and $d_{ss} = 0.66\ \mathrm{nm}$ the rise per base for ssDNA[44]. f_{ds} and f_{ss} are functions describing the extension-over-contour ratio for dsDNA and ssDNA, respectively, as a function of the applied force. For the dsDNA parts, we used an extensible worm-like-chain (eWLC) model, and for the ssDNA parts, a WLC model[45]. The persistence length was experimentally determined, for each molecule probed, by fitting force-extension curves.

Pause-free velocity calculation. The original, 2500 Hz data was low-pass filtered with a 3rd order Butterworth filter with a cutoff $f_c = 0.5\ Hz$, and the residency time in 1 bp windows, τ, was calculated. Data points corresponding to $\tau > med(\tau) + 5 \cdot mad(\tau)$, where $med(\tau)$ and $mad(\tau)$ are the median and the median absolute deviation of τ, respectively, were considered as belonging to pauses. Pauses shorter than 1s and polymerization bursts shorter than 2 bp, were discarded. The performance of the pause-detection scheme was tested using simulated traces[33], revealing ≤2% of false-negatives and ≤4% of false-positives across all the conditions tested[33]. The pause free velocity was calculated as the mean instantaneous velocity from the segments where the enzyme in not paused.

Fitting of the data. V_{max}, as a function of force, and PD_1, as a function of force and [dNTP], were globally fitted to their respective expressions, using Matlab's GlobalSearch, a scatter-search based global optimization method, running the solver fmincon. Confidence intervals for the fitted parameters were calculated by bootstrapping.

FUNDING

This work was supported by the Israel Science Foundation (Grant 1750/12 to AK), the Israeli Centers of Research Excellence program (I-CORE, Center no. 1902/12 to A.K), the European Commission (Grant 293923 to AK), and the Mallat Family Fund.

Author Contributions

A.K. designed and supervised the research. O.M. and H.K. performed the experiments. S.R. prepared reagents. O.M. and A.K. designed and built the optical tweezers setup. O.M., H.K. and A.K. analyzed the data. A.K. wrote the paper.

REFERENCES

1. Sarafianos, S. G. *et al.* Structure and Function of HIV-1 Reverse Transcriptase : Molecular Mechanisms of Polymerization and Inhibition. *J. Mol. Biol.* **385,** 693–713 (2009).

2. Kati, W. M., Johnson, K. A., Jerva, L. F. & Anderson, K. S. Mechanism and fidelity of HIV reverse transcriptase. *J. Biol. Chem.* **267,** 25988–97 (1992).

3. Reardon, J. E. Human Immunodeficiency Virus Reverse Transcriptase: Steady-State and Pre-Steady-State Kinetics of Nucleotide Incorporation. *Biochemistry* **31,** 4473–4479 (1992).

4. Reardon, J. E. Human immunodeficiency virus reverse transcriptase. A kinetic analysis of RNA-dependent and DNA-dependent DNA polymerization. *J. Biol. Chem.* **268,** 8743–51 (1993).

5. Zinnen, S., Hsieh, J. C. & Modrich, P. Misincorporation and mispaired primer extension by human immunodeficiency virus reverse transcriptase. *J. Biol. Chem.* **269,** 24195–202 (1994).

6. Kerr, S. G. & Anderson, K. S. Pre-steady-state kinetic characterization of wild type and 3'-azido-3'- deoxythymidine (AZT) resistant human immunodeficiency virus type 1 reverse transcriptase: Implication of RNA directed DNA polymerization in the mechanism of AZT resistance. *Biochemistry* **36,** 14064–14070 (1997).

7. Kellinger, M. W. & Johnson, K. A. Nucleotide-dependent conformational change governs specificity and analog discrimination by HIV reverse transcriptase. *Proc. Natl. Acad. Sci.* **107,** 7734–7739 (2010).

8. Avidan, O., Entin Meer, M., Oz, I. & Hizi, A. The processivity and fidelity of DNA synthesis exhibited by the reverse transcriptase of bovine leukemia virus. *Eur. J. Biochem.* **269,** 859–867 (2002).

9. Whiting, S. H. & Champoux, J. J. Strand displacement synthesis capability of Moloney murine leukemia virus reverse transcriptase. *J. Virol.* **68,** 4747–58 (1994).

10. Kamtekar, S. *et al.* Insights into Strand Displacement and Processivity from the Crystal Structure of the Protein-Primed DNA Polymerase of Bacteriophage φ29. *Mol. Cell* **16,** 609–618 (2004).

11. Manosas, M. *et al.* Mechanism of strand displacement synthesis by DNA replicative polymerases. *Nucleic Acids Res.* **40,** 6174–6186 (2012).

12. Morin, J. A. *et al.* Active DNA unwinding dynamics during processive DNA replication. *Proc. Natl. Acad. Sci.* **109,** 8115–8120 (2012).

13. Morin, J. A. *et al.* Mechano-chemical kinetics of DNA replication: identification of the translocation step of a replicative DNA polymerase. *Nucleic Acids Res.* **43,** 3643–3652 (2015).

14. Watts, J. M. *et al.* Architecture and secondary structure of an entire HIV-1 RNA genome. *Nature* **460,** 711–716 (2009).

15. Kelleher, C. D. & Champoux, J. J. Characterization of RNA strand displacement synthesis by Moloney murine leukemia virus reverse transcriptase. *J. Biol. Chem.* **273,** 9976–86 (1998).

16. Fuentes, G. M., Rodríguez-Rodríguez, L., Palaniappan, C., Fay, P. J. & Bambara, R. A. Strand displacement synthesis of the long terminal repeats by HIV reverse transcriptase. *J. Biol. Chem.* **271,** 1966–71 (1996).

17. Whiting, S. H. & Champoux, J. J. Properties of strand displacement synthesis by moloney murine leukemia virus reverse transcriptase: mechanistic implications. *J. Mol. Biol.* **278,** 559–577 (1998).

18. Sarafianos, S. G., Pandey, V. N., Kaushik, N. & Modak, M. J. Glutamine 151 participates in the substrate dNTP binding function of HIV-1 reverse transcriptase. *Biochemistry* **34,** 7207–16 (1995).

19. Spence, R. A., Kati, W. M., Anderson, K. S. & Johnson, K. A. Mechanism of inhibition of HIV-1 reverse transcriptase by nonnucleoside inhibitors. *Science* **267,** 988–93 (1995).

20. Huang, H., Chopra, R., Verdine, G. L. & Harrison, S. C. Structure of a Covalently Trapped Catalytic Complex of HIV-1 Reverse Transcriptase : Implications for Drug Resistance. *Science (80-.).* **1669,** (2009).

21. Sarafianos, S. G. *et al.* Lamivudine (3TC) resistance in HIV-1 reverse transcriptase involves steric hindrance with beta-branched amino acids. *Proc. Natl. Acad. Sci. U. S. A.* **96,** 10027–32 (1999).

22. Kirmizialtin, S., Nguyen, V., Johnson, K. A. & Elber, R. How Conformational Dynamics of DNA Polymerase Select Correct Substrates: Experiments and Simulations. *Structure* **20,** 618–627 (2012).

23. Steitz, T. A. & Steitz, J. A. A general two-metal-ion mechanism for catalytic RNA. *Proc. Natl. Acad. Sci. U. S. A.* **90,** 6498–502 (1993).

24. Castro, C. *et al.* Two proton transfers in the transition state for nucleotidyl transfer catalyzed by RNA- and DNA-dependent RNA and DNA polymerases. *Proc. Natl. Acad. Sci.* **104,** 4267–4272 (2007).

25. Bustamante, C., Chemla, Y. R., Forde, N. R. & Izhaky, D. Mechanical Processes in Biochemistry. *Annu. Rev. Biochem.* **73,** 705–748 (2004).

26. Abbondanzieri, E. A., Greenleaf, W. J., Shaevitz, J. W., Landick, R. & Block, S. M. Direct observation of base-pair stepping by RNA polymerase. *Nature* **438,** 460–5 (2005).

27. Sarafianos, S. G. *et al.* Structures of HIV-1 reverse transcriptase with pre- and post-translocation AZTMP-terminated DNA. *EMBO J.* **21,** 6614–24 (2002).

28. Marchand, B. & Götte, M. Site-specific Footprinting Reveals Differences in the Translocation Status of HIV-1 Reverse Transcriptase: IMPLICATIONS FOR POLYMERASE TRANSLOCATION AND DRUG RESISTANCE. *J. Biol. Chem.* **278,** 35362–35372 (2003).

29. Dangkulwanich, M. *et al.* Complete dissection of transcription elongation reveals slow translocation of RNA polymerase II in a linear ratchet mechanism. *Elife* **2,** e00971 (2013).

30. Betterton, M. D. & Jülicher, F. A Motor that Makes Its Own Track: Helicase Unwinding of DNA. *Phys. Rev. Lett.* **91,** 258103 (2003).

31. Kim, S., Schroeder, C. M. & Xie, X. S. Single-Molecule Study of DNA Polymerization Activity of HIV-1 Reverse Transcriptase on DNA Templates. *J. Mol. Biol.* **395,** 995–1006 (2010).

32. Manosas, M., Xi, X. G., Bensimon, D. & Croquette, V. Active and passive mechanisms of helicases. *Nucleic Acids Res. Reseach* **38,** 5518–5526 (2010).

33. Malik, O., Khamis, H., Rudnizky, S., Marx, A. & Kaplan, A. Pausing kinetics dominates strand-displacement polymerization by reverse transcriptase. *Nucleic Acids Res.* **42,** 434011 (2017).

34. Patel, P. H. *et al.* Insights into DNA polymerization mechanisms from structure and function analysis of HIV-1 reverse transcriptase. *Biochemistry* **34,** 5351–63 (1995).

35. Hsieh, J. C., Zinnen, S. & Modrich, P. Kinetic mechanism of the DNA-dependent DNA polymerase activity of human immunodeficiency virus reverse transcriptase. *J. Biol. Chem.* **268,** 24607–13 (1993).

36. Götte, M., Rausch, J. W., Marchand, B., Sarafianos, S. & Le Grice, S. F. J. Reverse transcriptase in motion: conformational dynamics of enzyme-substrate interactions. *Biochim. Biophys. Acta* **1804,** 1202–12 (2010).

37. Mizrahi, V., Henrie, R. N., Marlier, J. F., Johnson, K. A. & Benkovic, S. J. Rate-limiting steps in the DNA polymerase I reaction pathway. *Biochemistry* **24,** 4010–8 (1985).

38. Kuchta, R. D., Mizrahi, V., Benkovic, P. A., Johnson, K. A. & Benkovic, S. J. Kinetic mechanism of DNA polymerase I (Klenow). *Biochemistry* **26,** 8410–8417 (1987).

39. Doublié, S., Sawaya, M. R. & Ellenberger, T. An open and closed case for all polymerases. *Structure* **7,** R31–R35 (1999).

40. Johnson, K. A. Conformational Coupling in DNA Polymerase Fidelity. *Annu. Rev. Biochem.* **62,** 685–713 (1993).

41. Rudnizky, S. *et al.* H2A.Z controls the stability and mobility of nucleosomes to regulate expression of the LH genes. *Nat. Commun.* **7,** 12958 (2016).

42. Gittes, F. & Schmidt, C. F. Interference model for back-focal-plane displacement detection in optical tweezers. *Opt. Lett.* **23,** 7–9 (1998).

43. Berg-Sørensen, K. & Flyvbjerg, H. Power spectrum analysis for optical tweezers. *Rev. Sci. Instrum.* **75,** 594–612 (2004).

44. Huguet, J. M. *et al.* Single-molecule derivation of salt dependent base-pair free energies in DNA. *Proc. Natl. Acad. Sci. U. S. A.* **107,** 15431–6 (2010).

45. Marko, J. F. & Siggia, E. D. Stretching DNA. *Macromolecules* **28,** 8759–8770 (1995).

TABLES

Table 1: Force dependence of the Michaelis-Menten constants for the models tested.

	V_{max}	K_M
BR/B	$F\uparrow$	$F\downarrow$
BR/R	$F\uparrow$	$F\uparrow$
PS/B	–	$F\downarrow$
PS/R	$F\uparrow$	$F\uparrow$

* $F\uparrow$ ($F\downarrow$) indicates the parameter increases (decreases) with increasing force.

Table 2: Force dependence of the pause-density for the models tested.

	Pause origin			
	1	**2**	**3**	**4**
BR/B	$[T]\downarrow$, $F\downarrow$	$[T]\downarrow$	–	–
BR/R	$[T]\downarrow$	–	$F\downarrow$	–
PS/B	$[T]\downarrow$, $F\downarrow$	–	–	
PS/R	$[T]\downarrow$	–	$F\downarrow$	

* $F\uparrow$ ($F\downarrow$) indicates the parameter increases (decreases) with increasing force. $[T]\downarrow$ () indicates the parameter increases (decreases) with [dNTP]. – indicates force- and [dNTP] independence

Table 3: Microscopic rates obtained from fitting the pause-free velocity and PD

ΔG_{RT} (k_BT)	k_c (s^{-1})	k_t (s^{-1})	k_{-t} (s^{-1})	K_D (μM)	k_t (s^{-1})
0.87 ± 0.15	58 ± 37	22 ± 5	220 ± 145	0.4 ± 0.3	0.4 ± 0.1

* Shown are the estimated values and their 95% confidence interval

FIGURES CAPTIONS

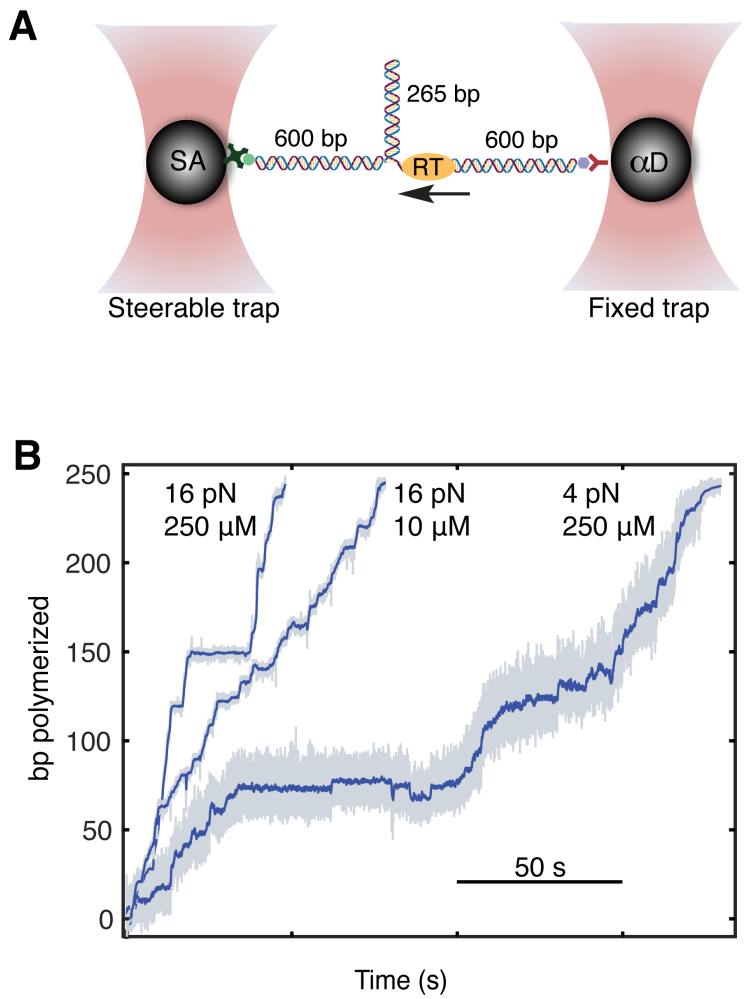

Figure 1: Following SD polymerization on a hairpin substrate under tension. (A) Experimental geometry. A 265 bp DNA hairpin is connected to two 600 bp dsDNA handles, and held under tension in a dual-trap optical tweezers. The 3'-OH terminus of one of the dsDNA handles serves as a primer for elongation (B) Time-traces of SD polymerization by RT. The extension of the tether is converted into the number of polymerized base pairs. Typical data is shown for different conditions of force and [dNTP].

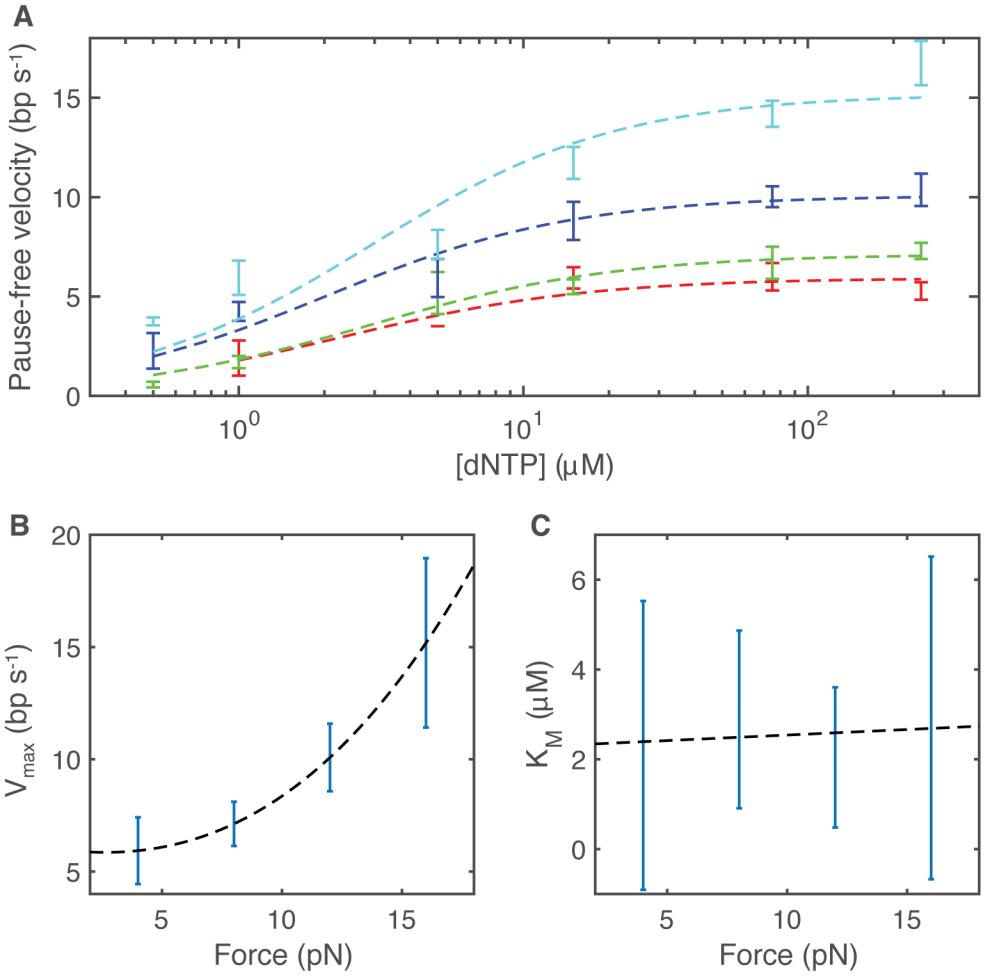

Figure 2: RT follows force-dependent Michaelis-Menten kinetics. (A) Pause free velocity for 4 (red), 8 (green), 12 (blue) and 16 (cyan) pN of force on the DNA. The pause free velocity was calculated, for a given force and [dNTP], by subtracting all pauses events in the polymerization trace. Data shown as mean ± sem. The dashed lines show the results of fits to the Michaelis Menten equation. (B) V_{max} as a function of the applied force. Shown are the estimated values from the fit, and their 95% confidence interval. (C) K_M as a function of the applied force. Shown are the estimated values from the fit, and their 95% confidence interval.

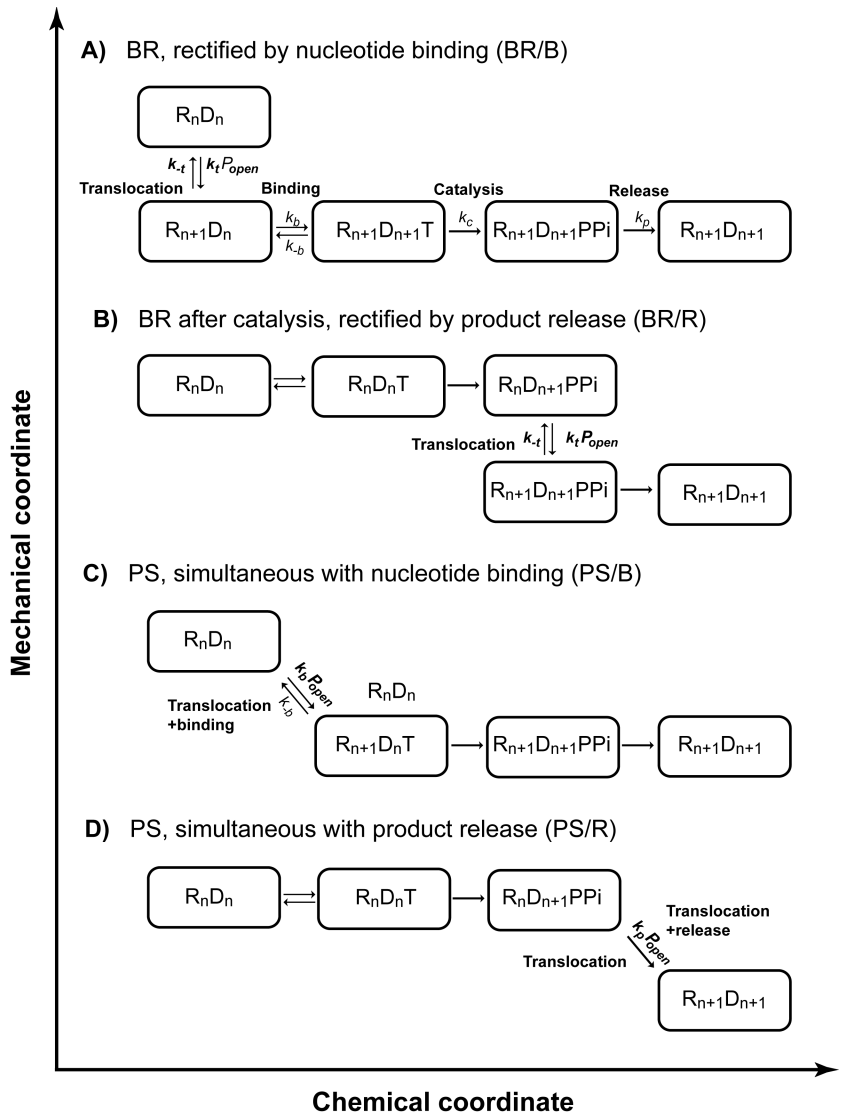

Figure 3: Different mechano-chemical schemes can incorporate a translocation step. Schematic description of the different mechano-chemical models used to predict the force- and [dNTP] dependence of the pause-free velocity. (A) A BR model, rectified by dNTP binding. (B) A PS model , where translocation is concomitant with dNTP binding. (C) A BR model, where dNTP releases locks the post-translocation state. (D) A PS model, with translocation occurring together with release of dNTP.

Supplementary Information

The mechano-chemistry of reverse transcriptase

Omri Malik[1,2,#], Hadeel Khamis[1,3,#], Sergei Rudnizky[1] and Ariel Kaplan[1,2,*]

[1]Faculty of Biology, Technion – Israel Institute of Technology, Haifa (32000), Israel
[2]Russell Berrie Nanotechnology Institute, Technion – Israel Institute of Technology, Haifa (32000), Israel
[3]Faculty of Physics, Technion – Israel Institute of Technology, Haifa (32000), Israel
* To whom correspondence should be addressed. Tel:+972-77-8871907; Fax: +972-7708871908; Email: akaplanz@technion.ac.il
# This authors contributed equally to this work

Supplementary discussion

Derivation of the kinetic constant for the models in Fig. 3

Model BR/B. A Brownian Ratchet, rectified by nucleotide binding:

This mechanism, similar to the one proposed for RNAP(1) and Phi29 DNA polymerase(2), and can be written as:

$$R_nD_n \underset{k_{-t}}{\overset{k_tP_{open}}{\leftrightarrow}} R_{n+1}D_n \underset{k_{-b}}{\overset{k_b[T]}{\leftrightarrow}} R_{n+1}D_nT \xrightarrow{k_c} R_{n+1}D_{n+1}PP_i \xrightarrow{k_p} R_{n+1}D_{n+1}$$

Using the net rate constants formalism(1, 3), or solving for the occupation probabilities in steady-state, it can be shown that the polymerization velocity, in bp/s, follows Michaelis-Menten (MM) kinetics, $V = V_{max}[T]/(K_M + [T])$, with:

$$V_{max} = \left[\frac{1}{k_p} + \frac{1}{k_c} + \frac{1}{k_tP_{open}}\right]^{-1} \text{ and } K_M = \frac{k_p(k_tP_{open}+k_{-t})(k_c+k_{-b})}{k_b(k_ck_p+k_tP_{open}k_c+k_tP_{open}k_p)}.$$

Assuming that catalysis is the rate limiting step, i.e. $k_c \ll k_p, k_{-b}, k_t, k_{-t}$, and using the notation $K_D = \frac{k_{-b}}{k_b}$, $K_\delta \equiv \frac{k_{-t}}{k_t}$, and $K_D \equiv \frac{k_{-b}}{k_b}$, we can write:

$$V_{max} = \left[\frac{1}{k_c} + \frac{1}{k_tP_{open}}\right]^{-1} \text{ and } K_M \approx K_D\frac{(k_tP_{open}+k_{-t})}{(k_tP_{open}+k_c)} = K_D\frac{1+\frac{K_\delta}{P_{open}}}{1+\frac{k_c}{k_tP_{open}}}.$$

Model BR/R. A Brownian Ratchet after catalysis, rectified by product release

The scheme for this model is described by

$$R_nD_n \underset{k_{-b}}{\overset{k_b[T]}{\leftrightarrow}} R_nD_nT \xrightarrow{k_c} R_nD_{n+1}P_i \underset{k_{-t}}{\overset{k_tP_{open}}{\leftrightarrow}} R_{n+1}D_{n+1}PP_i \xrightarrow{k_p} R_{n+1}D_{n+1}$$

which results in $V_{max} = \left[\frac{1}{k_c} + \frac{1}{k_p} + \frac{k_p+k_{-t}}{k_pk_tP_{open}}\right]^{-1}$ and $K_M = \frac{k_pk_tP_{open}(k_c+k_{-b})}{k_b(k_ck_p+k_ck_{-t}+k_tP_{open}k_c+k_tP_{open}k_p)}$

With the same assumptions as before, we get: $V_{max} = \left[\frac{1}{k_c} + \frac{k_p+k_{-t}}{k_pk_tP_{open}}\right]^{-1} = \left[\frac{1}{k_c} + \frac{1}{k_t^{net}P_{open}}\right]^{-1}$

And $K_M = K_D\frac{k_pk_tP_{open}}{k_ck_p+k_ck_{-t}+k_tP_{open}k_p} = K_D\left[\frac{k_c(k_p+k_{-t})}{k_pk_tP_{open}} + 1\right]^{-1} = K_D\left[1 + \frac{k_c}{k_t^{net}P_{open}}\right]^{-1}$

where we have used the definition $\mathrm{k_t^{net}} = \frac{\mathrm{k_pk_t}}{\mathrm{k_p+k_{-t}}}$.

Model PS/B. A Power Stroke, simultaneous with nucleotide binding

The cycle in this case is described by:

$$R_nD_n \underset{k_{-b}}{\overset{k_b[T]P_{open}}{\leftrightarrow}} R_{n+1}D_nT \overset{k_c}{\rightarrow} R_{n+1}D_{n+1}PP_i \overset{k_p}{\rightarrow} R_{n+1}D_{n+1}$$

which results in $V_{max} = \left[\frac{1}{k_c} + \frac{1}{k_p}\right]^{-1}$ and $K_M = \frac{k_p(k_c+k_{-b})}{k_bP_{open}(k_c+k_p)}$.

With the usual approximations, we get: $V_{max} = k_c$ and $K_M = \frac{K_D}{P_{open}}$.

Model PS/R. A Power Stroke, simultaneous with product release

$$R_nD_n \underset{k_{-b}}{\overset{k_b[T]}{\leftrightarrow}} R_nD_nT \overset{k_c}{\rightarrow} R_nD_{n+1}P_i \overset{k_pP_{open}}{\rightarrow} R_{n+1}D_{n+1}$$

which results in $V_{max} = \left[\frac{1}{k_c} + \frac{1}{k_pP_{open}}\right]^{-1}$ and $K_M = \frac{k_pP_{open}(k_c+k_{-b})}{k_b(k_c+k_pP_{open})}$,

and is approximated as $V_{max} = \left[\frac{1}{k_c} + \frac{1}{k_pP_{open}}\right]^{-1} = k_c\left[1 + \frac{k_c}{k_pP_{open}}\right]^{-1}$ and $K_M = K_D\left[1 + \frac{k_c}{k_pP_{open}}\right]^{-1}$

All the calculated expression above are summarized in Supplementary Table 4.

Calculation of pause probability and pause density

We define PD_j as the probability, per cycle, to enter a pause from state j. It can be calculated by looking at the rate of entering the paused state from state j vs. the rate of productively continuing the cycle. We caracterize this last rate by k_j^{net} and therefore $PD_j = \frac{k_{pause}}{k_{pause}+k_j^{net}}$

where k_{pause} is the intrinsic rate of entering the pause. Hence, to calculate PDs we need first to calculate k_j^{net} for the specific state of origin.

Model BR/B. A Brownian Ratchet, rectified by nucleotide binding

In the case of model BR/B, the pause can be entered from 4 different kinetic states: the pre-translocation state, the post-translocated state (before dNTP binding), the dNTP bound state, and the post-catalysis state, before Pi release. It can be shown that,

$$k_1^{net} = \frac{k_b[T]k_t P_{open} k_c}{k_{-t}(k_c + k_{-b}) + k_b[T]k_c}$$

and under the assumptions that k_c is the rate limiting step, as before,

$$k_1^{net} \approx \left[\frac{K_\delta}{P_{open}}\frac{K_D}{[T]}\frac{1}{k_c} + \frac{1}{k_t P_{open}}\right]^{-1} = k_t P_{open}\left[\left(1 + \frac{k_{-t}}{k_c}\frac{K_D}{[T]}\right)\right]^{-1}$$

in the same way we can calculate $k_2^{net} = \frac{k_b[T]k_c}{k_c+k_{-b}} = \frac{[T]}{K_D}k_c$, $k_3^{net} = k_c$, and $k_4^{net} = k_p$.

Hence, the calculated PDs are given by:

$$PD_1 = \frac{k_{pause}}{k_{pause} + k_t P_{open}\left[\left(1 + \frac{k_{-t}}{k_c}\frac{K_D}{[T]}\right)\right]^{-1}} = \left[1 + \frac{k_t P_{open}}{k_{pause}}\left[\left(1 + \frac{k_{-t}}{k_c}\frac{K_D}{[T]}\right)\right]^{-1}\right]^{-1}$$

$$PD_2 = \frac{k_{pause}}{k_{pause} + \frac{[T]}{K_D}k_c} = \left[1 + \frac{[T]}{K_D}\frac{k_c}{k_{pause}}\right]^{-1}$$

$$PD_3 = \frac{k_{pause}}{k_{pause} + k_c}$$

and

$$PD_4 = \frac{k_{pause}}{k_{pause} + k_p}$$

Model BR/R. A Brownian Ratchet after catalysis, rectified by product release

$k_1^{net} = \frac{k_b[T]k_c}{k_c+k_{-b}} \approx \frac{k_b[T]k_c}{k_{-b}} = \frac{[T]}{K_D}k_c$, $k_2^{net} = k_c$,

$k_3^{net} = \frac{k_t P_{open} k_p}{k_p + k_{-t}} = k_t P_{open} \left[1 + \frac{k_{-t}}{k_p}\right]^{-1}$, and $k_4^{net} = k_p$.

And therefore:

$$PD_1 = \frac{k_{pause}}{k_{pause} + \frac{[T]}{K_D} k_c}$$

$$PD_2 = \frac{k_{pause}}{k_{pause} + k_c}$$

$$PD_3 = \frac{k_{pause}}{k_{pause} + k_t P_{open} \left[1 + \frac{k_{-t}}{k_p}\right]^{-1}}$$

$$PD_4 = \frac{k_{pause}}{k_{pause} + k_p}$$

Model PS/B. A Power Stroke, simultaneous with nucleotide binding

$k_1^{net} = \frac{k_b [T] P_{open} k_c}{k_c + k_{-b}} \approx \frac{k_b [T] P_{open} k_c}{k_{-b}} = \frac{[T] P_{open}}{K_D} k_c$, $k_2^{net} = k_c$ and $k_3^{net} = k_p$. Hence,

$$PD_1 = \frac{k_{pause}}{k_{pause} + \frac{[T] P_{open}}{K_D} k_c}$$

$$PD_2 = \frac{k_{pause}}{k_{pause} + k_c}$$

$$PD_3 = \frac{k_{pause}}{k_{pause} + k_p}$$

Model PS/R. A Power Stroke, simultaneous with product release

$k_1^{net} = \frac{k_b [T] k_c}{k_c + k_{-b}} \approx \frac{k_b [T] k_c}{k_{-b}} = \frac{[T]}{K_D} k_c$, $k_2^{net} = k_c$ and $k_3^{net} = k_p P_{open}$. Hence,

$$PD_1 = \frac{k_{pause}}{k_{pause} + \frac{[T]}{K_D} k_c}$$

$$PD_2 = \frac{k_{pause}}{k_{pause} + k_c}$$

$$PD_3 = \frac{k_{pause}}{k_{pause} + k_p P_{open}}$$

All the calculated PDs are summarized in Supplementary Table 5.

Calculation of P_{open}

As was shown in the previous section, the different models exhibit different dependencies on P_{open}, both for the MM parameters and for the PD. Since P_{open} is expected to depend on the applied force, the sequence and, possibly, some degree of destabilization provided by the enzyme, the next step in order to describe force dependence of the velocity is to calculate P_{open}. A thermodynamic calculation of P_{open} should take into account the fact that, in our setup, the distance between the traps, X_T, is the externally controlled parameter, and that all other parameters (the tension on the tether, its total extension and the extension of each of its components) are, in equilibrium, fluctuating variables (this has been called(4, 5) the "mixed-ensemble"). Our experimental setup is composed of several compliant elements, or "springs", in series: A bead in the harmonic potential of the fixed trap, a dsDNA handle, the ssDNA that was "released" from previous rounds of polymerization, the dsDNA that was polymerized in the previous rounds, a second dsDNA handle, and a bead in the harmonic potential of the steerable trap. We can simplify this picture by collecting together similar term to result in an effective model composed of a single, effective trapping potential with stiffness $k_{trap}^{-1} = k_{t_1}^{-1} + k_{t_2}^{-1}$ (k_{t_1} and k_{t_2} are the measured spring-constant for the two traps), a ssDNA portion of length m and a dsDNA portion of length $N_H + m$, which are connected to a hairpin with size $N_{HP} - m$. Here, m is the number of bps that were unwound and polymerized in previous rounds, $N_H$is the length (number of bps) of the dsDNA handle, and N_{HP} the total number of bps in the hairpin, before polymerization.

For a given F and m, we assume the system is in contact, and in equilibrium, with the thermal bath, and therefore will explore different k-states (i.e. states with additional k bps open) and populate them with a probability P_k according to a Boltzmann distribution, $P_k(F,m) = Z^{-1}\exp\left(-\beta \cdot \Delta G_k(F,m)\right)$, where $Z(F,m) = \sum_{j=0}^{N_{HP}-m} \exp\left(-\beta \cdot \Delta G_j(F)\right)$ is the partition function and $\beta \equiv 1/(k_B T)$. The probability of a *productive* opening state, i.e. an opening equal or greater than the size of the enzyme's step, is given by $P_{open}(s,F,m) = \sum_{k=s}^{N_{HP}-m} P_k(F,m)$. Hence, calculating P_{open} is reduced to calculating $\Delta G_k(F,m)$ for the given force on the tether and the number of previously polymerized bps. As was shown before(4, 6), there are three contributions to ΔG_k: i) The base-pairing energy $\Delta G_{bp}(k)$, that results from the stacking and hydrogen bonding that are disrupted during opening; ii) a force-dependent contribution $\Delta G_F(k;F,m)$ that results from the k-dependent changes in equilibrium configuration of the different "springs" in the system; and iii) a possible destabilization energy ΔG_{RT} contributed by RT. In summary, $\Delta G_k = \Delta G_{bp}(k) + \Delta G_F(k,F) + \Delta G_{RT}$.

Following is the calculation of each of these terms.

Calculation of $\Delta G_{bp}(k)$. The difference in base-pairing free-energy between the closed state ($k = 0$) and an arbitrary k state where k bps have been disrupted, can be written as $\Delta G_{bp}(k) = \sum_{j=1}^{k} E_j^{NN}$, where $E_j^{NN}$is the base-pairing energy of element j in the hairpin. It is calculated in the

framework of the nearest-neighbor model(7), for our experimental salt concentration, using a recently improved set of values(8). Since we measure the mean velocity over the full hairpin, we can use $\Delta G_{bp}(k) \approx k \cdot \langle E^{NN} \rangle$, where $\langle E^{NN} \rangle$ is the weighted average of E_k^{NN} over our specific sequence. For our case, $\langle E^{NN} \rangle = -2.38\ k_B T$.

Calculation of $\Delta G_F(k)$. We wish to calculate the free energy difference between state k, with k bps open, and the closed state, $k = 0$, i.e. $\Delta G_F(k) = G(k) - G(0)$. We use the fact that the distance between the traps, and therefore the sum of all the contributions to the extension, is constant. Hence, for the closed state (k=0) we can express the distance between the traps as:

$$X_T = (N_H + m) \cdot d_{ds} \cdot x_{ds}(F) + m \cdot d_{ss} \cdot x_{ss}(F) + \frac{F}{k_{trap}}$$

where d_{ds} is the rise per bp for dsDNA, and d_{ss} the rise per base for ssDNA. x_{ds}(F) and $x_{ss}(F)$ represent the ratio of the extension of the polymer to its contour length, i.e. they are the inverse of the thermodynamic force-extension curves that characterize dsDNA and ssDNA, ($f_{ss}(x)$ and $f_{ss}(x)$, respectively). In our experiment, these are an Extensible Worm Like Chain for dsDNA, and Worm Like Chain for ssDNA, with experimentally determined parameters.

If k bps open, $2k$ nts of ssDNA are added to the total extension and, in addition, the force on the tether is no longer F, but $F + \Delta F(k;\ F, m)$. The distance between the traps, however, remains the same. Hence,

$$X_T = (N_H + m) \cdot d_{ds} \cdot x_{ds}(F + \Delta F) + (m + 2k) \cdot d_{ss} \cdot x_{ss}(F + \Delta F) + \frac{F + \Delta F}{k_{trap}}$$

Since the two extensions calculated must be equal, these equations uniquely determine $\Delta F(k;\ F, m)$ (Supplementary Fig. 1a).

Once $\Delta F(k;\ F, m)$ is known, we can calculate, for each of the "springs" in series, its k-dependent extension, and then its contribution to the free energy change. The differences in free energy can be written as:

$$\Delta G_F = G(k, m; F + \Delta F) - G(0, m; F) = \Delta G_t + \Delta G_d + \Delta G_{s1} + \Delta G_{s2}$$

where ΔG_t is the work done by the movement of the beads in the traps, ΔG_d is the work of changing the stretching of the dsDNA (handles + previously polymerized), ΔG_{s1} the work of changing the stretching of the previously release ssDNA, and ΔG_{s2} is the work performed to stretch the newly release ssDNA from zero force to the final force. I.e.,

$$\Delta G_t = \int_{x_b(F)}^{x_b[F+\Delta F(k;F,m)]} F_b(x')dx' = \int_{x_b(F)}^{x_b[F+\Delta F(k;F,m)]} k_t \cdot x' dx'$$

$$\Delta G_d = (N_H + m) \cdot d_{ds} \cdot \int_{x_{ds}(F)}^{x_{ds}[F+\Delta F(k;F,m)]} f_{ds}(x')dx'$$

$$\Delta G_{s1} = m \cdot d_{ss} \cdot \int_{x_{ss}(F)}^{x_{ss}[F+\Delta F(k;F,m)]} f_{ss}(x')dx'$$

$$\Delta G_{s2} = 2k \cdot d_{ss} \cdot \int_0^{x_s[F+\Delta F(k;F,m)]} f_{ss}(x')dx'$$

All these contributions are calculated numerically and summed to calculate ΔG_F (Supplementary Fig. 1b-f). Having calculated ΔG_F and ΔG_{bp}, we can now, for any value of ΔG_{RT}, calculate ΔG_k, P_k and finally P_{open} (Supplementary Fig. 1g-i).

References

1. Dangkulwanich,M., Ishibashi,T., Liu,S., Kireeva,M.L., Lubkowska,L., Kashlev,M. and Bustamante,C.J. (2013) Complete dissection of transcription elongation reveals slow translocation of RNA polymerase II in a linear ratchet mechanism. *Elife*, **2**, e00971.

2. Morin,J.A., Cao,F.J., Lazaro,J.M., Arias-Gonzalez,J.R., Valpuesta,J.M.J.M., Carrascosa,J.L.J.L., Salas,M., Ibarra,B., Lázaro,J.M., Ricardo Arias-Gonzalez,J., *et al.* (2015) Mechano-chemical kinetics of DNA replication: identification of the translocation step of a replicative DNA polymerase. *Nucleic Acids Res.*, **43**, 3643–3652.

3. Cleland,W.W. (1975) Partition analysis and concept of net rate constants as tools in enzyme kinetics. *Biochemistry*, **14**, 3220–3224.

4. Manosas,M. and Ritort,F. (2005) Thermodynamic and kinetic aspects of RNA pulling experiments. *Biophys. J.*, **88**, 3224–42.

5. Manosas,M., Wen,J.-D., Li,P.T.X., Smith,S.B., Bustamante,C., Tinoco,I. and Ritort,F. (2007) Force unfolding kinetics of RNA using optical tweezers. II. Modeling experiments. *Biophys. J.*, **92**, 3010–21.

6. Johnson,D.S., Bai,L., Smith,B.Y., Patel,S.S. and Wang,M.D. (2007) Single-Molecule Studies Reveal Dynamics of DNA Unwinding by the Ring-Shaped T7 Helicase. *Cell*, **129**, 1299–1309.

7. SantaLucia,J. (1998) A unified view of polymer, dumbbell, and oligonucleotide DNA nearest-neighbor thermodynamics. *Proc. Natl. Acad. Sci. U. S. A.*, **95**, 1460–5.

8. Huguet,J.M., Bizarro,C. V, Forns,N., Smith,S.B., Bustamante,C. and Ritort,F. (2010) Single-molecule derivation of salt dependent base-pair free energies in DNA. *Proc. Natl. Acad. Sci. U. S. A.*, **107**, 15431–6.

9. Malik,O., Khamis,H., Rudnizky,S., Marx,A. and Kaplan,A. (2017) Pausing kinetics dominates strand-displacement polymerization by reverse transcriptase. *Nucleic Acids Res.*, **42**, 434011.

Supplementary Figures:

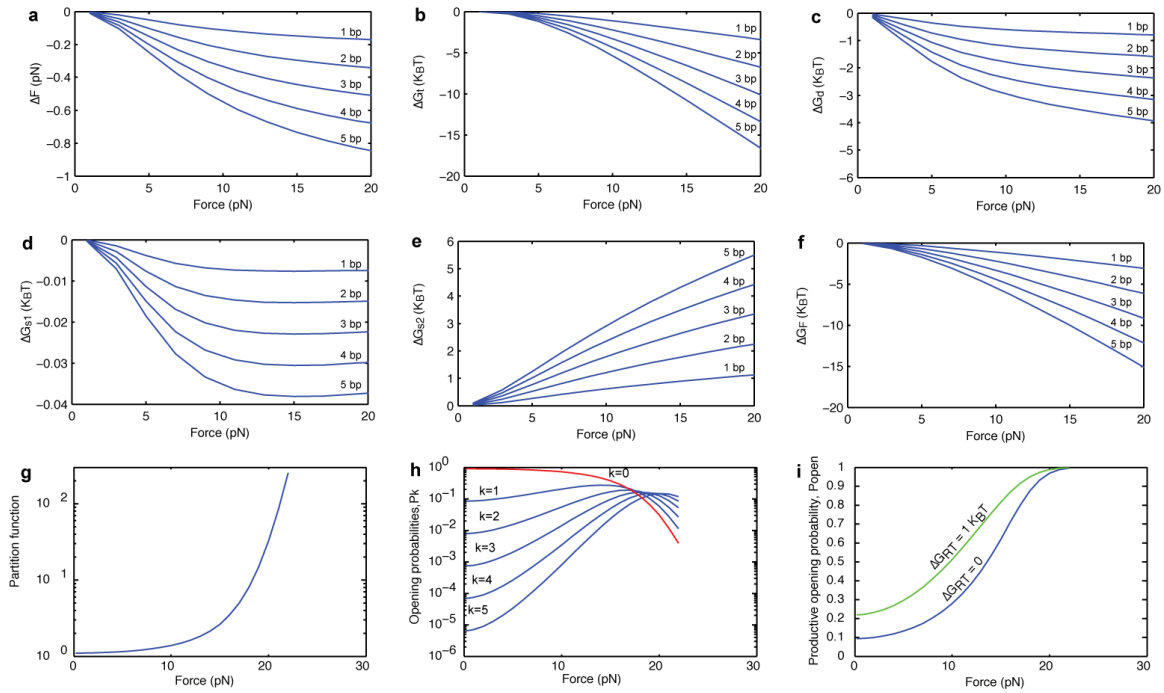

Supplementary Figure 1: Calculation of Popen. (a-f) Different contributions to the free energy of opening a fork under tension. (a) Changes in force us the forks open, as a function of the initial force. (b) Free-energy change contributed by movement of the bead in the trap. (c) Contribution of dsDNA stretching. (d) Contribution of stretching the ssDNA present from previous cycles. (e) Contribution of stretching the newly released ssDNA. (f) Sum of all contributions. (a-f) Only 5 possible states (1-5 bp open) are shown for clarity.

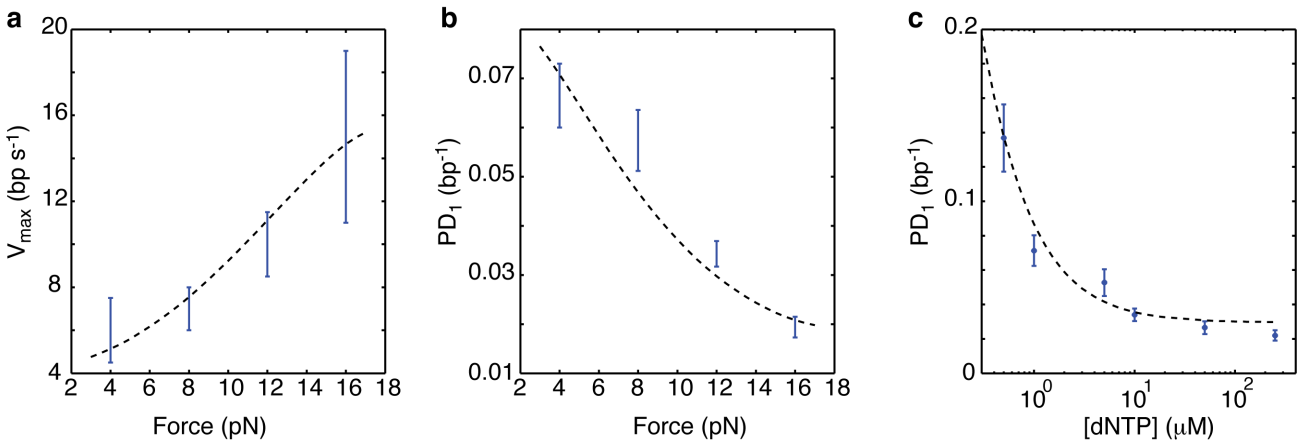

Supplementary Figure 2: Global fitting of V_{max} and PD_1, in the BR/B model. Simultaneously fitting V_{max} as a function of force (a), PD_1 as a function of force, for [dNTP]=250uM (b), and PD_1 as a function of [dNTP], for F=12 pN (c), to their respective expressions allows us to find ΔG_{RT} and the microscopic rates shown in Table 3. The data in b and c is taken from Ref. (9)

Supplementary Tables:

Supplementary Table 1: Complete polymerization construct

Sequence (5'→3')
ggtcatcgctgaggggcaagctgaggcgtagTGCCGGCCGATGGACCCTATACGCGGCCGCCCTGGAGAATCCCGGTGCCGAGGCCGCTCAATTGGTCGTAGCAAGCTCTAGCACCGCTTAAACGCACGTACGCGCTGTCCCCCGCGTTTTAACCGCCAAGGGGATTACTCCCTAGTCTCCAGGCACGTGTCAGATATATACATCCTGTGCATGTATTGAACAGCGACCTTCTCGGGGATATCGAATTCCACGCAGACTTGAGGCAA

(*) The last AA in both sequences is not paired

Supplementary Table 2: Primers used for templates PCR reactions

DNA origin	Incorporated restriction enzyme site	Primer sequence (5'→3')
"601" nucleosome positioning sequence	BglI	ATGGCCTTGCCGGCCGATGGACCCTATACGCGGCC
	DraIII	ATCACTGCGTGGAATTCGATATCCCCGAGAAGG

Supplementary Table 3: Primers used for handles PCR reactions

Name	Primer/modification	Primer sequence (5'→3')
Biotin handle	F (5'-biotin)	GCTTTAATGCGGTAGTTTATCA
	R (Nt.BbVCI)	GCAGCATTAGGAAGCAGCCCAGGCATTAGGAAGCAGCCCAG
Dig handle	F (5'-phosphate/Nb.BbvCI)	GCATTAGGAAGCAGCCCAGGCTTTATTGCGGTAGTTTATCA
	R (5'-digoxigenin)	GCATTAGGAAGCAGCCCAG

Supplementary Table 4: Michaelis-Menten constants for the models tested

	V_{max}	K_M	**Free parameters**
B1	$\left[\frac{1}{k_c}+\frac{1}{k_t P_{open}}\right]^{-1}$	$K_D \frac{1+\frac{K_\delta}{P_{open}}}{1+\frac{k_c}{k_t P_{open}}}$	k_c, k_t, k_{-t}, K_D
B3	$\left[\frac{1}{k_c}+\frac{1}{k_t^{net} P_{open}}\right]^{-1}$	$K_D\left[1+\frac{k_c}{k_t^{net} P_{open}}\right]^{-1}$	k_c, k_t^{net}, K_D
P1	k_c	$\frac{K_D}{P_{open}}$	k_c, K_D
P2	$\left[\frac{1}{k_c}+\frac{1}{k_p P_{open}}\right]^{-1}$	$K_D\left[1+\frac{k_c}{k_p P_{open}}\right]^{-1}$	k_c, k_p, K_D

Supplementary Table 5: Calculated density of pauses, as a function of the kinetic model and the pause origin.

	Pause origin			
	1	**2**	**3**	**4**
B1	$\frac{k_{pause}}{k_{pause}+k_t P_{open}\left[\left(1+\frac{k_{-t}}{k_c}\frac{K_D}{[T]}\right)\right]^{-1}}$	$\frac{k_{pause}}{k_{pause}+\frac{[T]}{K_D}k_c}$	$\frac{k_{pause}}{k_{pause}+k_c}$	$\frac{k_{pause}}{k_{pause}+k_p}$
B3	$\frac{k_{pause}}{k_{pause}+\frac{[T]}{K_D}k_c}$	$\frac{k_{pause}}{k_{pause}+k_c}$	$\frac{k_{pause}}{k_{pause}+k_t^{net}P_{open}}$	$\frac{k_{pause}}{k_{pause}+k_p}$
P1	$\frac{k_{pause}}{k_{pause}+\frac{[T]P_{open}}{K_D}k_c}$	$\frac{k_{pause}}{k_{pause}+k_c}$	$\frac{k_{pause}}{k_{pause}+k_p}$	
P2	$\frac{k_{pause}}{k_{pause}+\frac{[T]}{K_D}k_c}$	$\frac{k_{pause}}{k_{pause}+k_c}$	$\frac{k_{pause}}{k_{pause}+k_p P_{open}}$	